Applied Catalysis A: General 458 (2013) 28–38

Contents lists available at SciVerse ScienceDirect

Applied Catalysis A: General

journal homepage: www.elsevier.com/locate/apcata

Liquid-phase dehydration of 1-phenylethanol on solid acids: Influence of catalyst acidity and pore structure

Nicolás M. Bertero, Andrés F. Trasarti, Carlos R. Apesteguía, Alberto J. Marchi*

Catalysis Science and Engineering Research Group (GICIC), Instituto de Investigaciones en Catálisis y Petroquímica (INCAPE), UNL-CONICET, Santiago del estero 2654, 3000 Santa Fe, Argentina

ARTICLE INFO

Article history:
Received 13 January 2013
Received in revised form 13 March 2013
Accepted 16 March 2013
Available online xxx

Keywords:
Liquid-phase dehydration
Acid catalysis
Shape selectivity
1-Phenylethanol
Styrene

ABSTRACT

The liquid-phase dehydration of 1-phenylethanol (PHE) over different solid acids was studied at 363 K using cyclohexane as solvent. It was found that the catalyst activity and selectivity strongly depended on: (1) the nature, strength and density of acid sites and (2) the textural properties of the catalyst.

Catalysts containing mainly surface Brønsted acid sites of medium–high strength, such as Amberlyst 15, HPA/SiO_2, and HMOR zeolite, showed low initial styrene (STY) selectivity because the PHE dehydrated to alpha-methylbenzyl ether (AME) at higher or similar rates than to STY. Both primary products, STY and AME, were consecutively transformed to other heavy products (HP).

Catalysts containing predominantly Lewis acid sites, such as ZnO/SiO_2, Al-MCM-41 and SiO_2–Al_2O_3, selectively transformed PHE to AME. The ether can be sequentially converted to STY and HP, depending on the solid acidity. Solid acids having strong surface Lewis sites, e.g. SiO_2–Al_2O_3, showed high dehydration rate and HP production. Samples containing exclusively weak Lewis acid sites, e.g. γ-Al_2O_3, were not active in the PHE dehydration at 363 K.

Only zeolites HZSM-5, HBEA and HY, with similar surface density of Brønsted and Lewis acid sites, converted selectively PHE into STY, giving initial STY selectivities between 83 and 96%. However, HY zeolite was rapidly deactivated due to the blockage of its microporous structure by bulky compounds formed inside the large cages of 13 Å. Instead, on HBEA, STY was converted to HP that can diffuse through the solid microporous structure. Then, the selectivity to STY was drastically reduced with time. A constant and high STY selectivity at total PHE conversion was only obtained with HZSM-5. The pore size of this zeolite is enough to allow the diffusion and conversion of PHE into STY, but it is not adequate to form the surface intermediates leading to AME and HP.

Thus, it was proved that: (1) the surface Brønsted to Lewis ratio strongly influences the initial selectivity in the liquid-phase PHE dehydration; (2) a similar Brønsted to Lewis ratio on the solid acid surface is necessary to obtain high initial selectivity to STY; and (3) the right porous structure is crucial to avoid HP production and keep constant the STY selectivity at high PHE conversion. From the experimental results obtained in this work, a mechanistic approach was proposed in order to explain the influence of both acid site nature and pore size on the selective PHE dehydration in liquid phase.

1. Introduction

One powerful and usual method to obtain olefins in the chemical industry is the alcohol dehydration, which can be performed in either gas or liquid phase. On the one hand, gas phase dehydration of alcohols is a relatively benign process for the environment that was traditionally carried out using titania [1], alumina [2–4], silica–alumina [5] or zeolites [6,7] as catalysts, at temperatures higher than 473 K. On the other hand, liquid-phase alcohol dehydration is generally carried out using traditional homogeneous catalysis, comprising strong acids such as H_2SO_4, $KHSO_4$, H_3PO_4 or p-toluensulfonic acid [8–10]. This technology has severe drawbacks during both chemical reaction and catalyst recovering-reuse, such as generation of large amount of byproducts, high energy demand, serious corrosion in equipments and environmental problems due to catalyst leakages [11]. Consequently, it is of great importance to find new active and selective catalysts for eco-friendly liquid-phase alcohol dehydration. The main advantages of heterogeneous catalysis over its homogeneous counterpart are: (1) reduced equipment corrosion; (2) easy product and catalyst separation; (3) low-cost recycle of catalysts; and (4) less contamination in waste streams due to leakages of catalyst. Thus, heterogeneous catalysis offer relevant possibilities for sustainable olefin

* Corresponding author. Tel.: +54 342 4571164; fax: +54 342 4531068.
E-mail addresses: amarchi@fiq.unl.edu.ar, albertojuliomarchi@gmail.com (A.J. Marchi).

0926-860X/$ – see front matter © 2013 Elsevier B.V. All rights reserved.
http://dx.doi.org/10.1016/j.apcata.2013.03.018

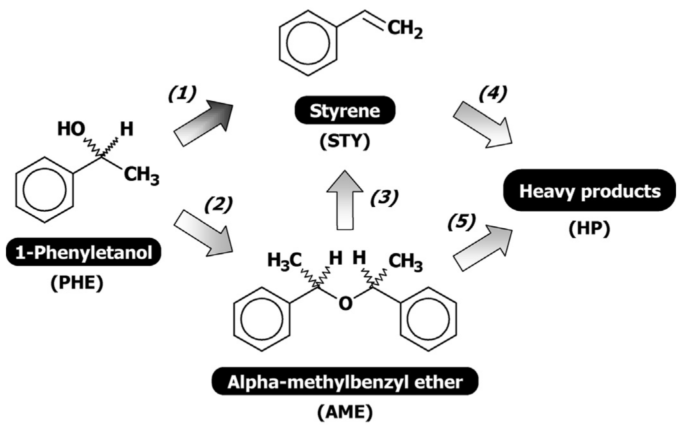

Fig. 1. Reaction scheme for the 1-phenylethanol dehydration over acidic catalysts.

production, replacing environmental hazardous homogeneous catalysis by processes that use solid acid catalysts [11,12].

In particular, intramolecular dehydration of 1-phenylethanol (PHE), a secondary aromatic alcohol, is of industrial interest in order to produce styrene (STY). This is a well-known reaction, because 15% of the worldwide STY is produced by PHE dehydration, which is a byproduct obtained in the production of propylene oxide [13]. The PHE dehydration process is the most used when high purity STY is needed [5]. This olefin is used as raw material for the production of a wide variety of polymeric products, specially thermoplastics and elastomers, to produce goods such as furnitures, tanks, toys, etc. [14]. The liquid-phase PHE dehydration is also used as test reaction for the synthesis of fine chemicals, such as indenes from indanols, widely used for the production of pharmaceuticals and polymerization catalysts [15–18]. Besides STY, and depending on the catalyst and operational conditions, alpha-methylbenzyl ether (AME) can also be a primary product formed through intermolecular PHE dehydration (Fig. 1). Both AME and STY can lead consecutively to the formation of heavy products (HP) over acidic catalysts.

PHE dehydration in liquid phase using solid catalysts such as Al_2O_3, SiO_2–Al_2O_3, zeolites or acidic resins have been reported in previous works [19–24]. In all the cases, the reaction temperature was always higher than 423 K. In general, selectivity to STY was between 74 and 98%, depending on the experimental conditions, though some deactivation of the catalyst took place. Lange and Otten studied the PHE dehydration under reactive distillation conditions over microporous and mesoporous solid acids at 443 K [22,23]. These authors remarked the importance of the shape selectivity for obtaining high STY selectivity and observed important deactivation of the catalysts. Recently, Pérez Valencia et al. reported the selective 1-phenylethanol dehydration at temperatures between 398 and 460 K using 1-methylimidazolium hydrogen sulfate as catalyst in a bubble column reactor [25]. Only few papers dealing with the liquid-phase dehydration of PHE at temperature lower than 373 K have been published [26–28]. Tarlani et al. dehydrated PHE at 353 K over $H_6P_2W_{12}O_{62}$ using dichloroethylene as solvent, but they obtained mostly HP and only traces of STY [26]. In previous works, we have reported the successful use of zeolites for the selective PHE liquid-phase dehydration at 363 K [27,28]. Dealuminated mordenite-like zeolites were more selective to STY than to AME, though their microporous structure allows the formation of bulky products [27]. On the other hand, STY selectivities higher than 92% were obtained over HZSM-5 and a mechanistic LHHW kinetic model was proposed to interpret the results [28]. On the basis of the information found in the open literature, it was concluded that a more systematic and exhaustive study is necessary in order to explain the very changing selectivity to styrene obtained with the different solid acids mentioned above.

From an industrial point of view, the successful use of solid acid catalysts for eco-friendly processes is based on the understanding of the influence of both acid and textural properties on the selectivity. To our knowledge, there is very little information in the open literature in which the influence of acidity and pore structure on the selective liquid-phase PHE dehydration under mild conditions was studied. In this work the liquid-phase dehydration of PHE was carried out at 363 K using cyclohexane as solvent, employing several selected acidic solids having different nature, strength and density of acid sites and with markedly different textural properties. The aim is to investigate the influence of acidity and porous structure on the PHE dehydration rate and selectivity to STY. To achieve this aim, mesoporous and microporous solids belonging to one of the following three categories were employed as catalysts for the liquid-phase PHE dehydration: (1) solid acids having mainly surface Lewis acid sites; (2) solid acids having mainly surface Brønsted acid sites; (3) solid acids having similar proportions of Brønsted and Lewis acid sites on the surface. It was found out that high initial selectivity to STY is obtained only when solids with similar surface concentrations of Lewis and Brønsted acid sites are used as catalysts. However, this high selectivity was preserved only if the pore size is such that conversion of STY into HP can be inhibited. On the basis of the experimental results obtained in this work, a mechanistic approach was finally proposed in order to explain the influence of both acid site nature and pore size on the selective PHE dehydration in liquid phase. The final goal is to determine the requirements to perform an eco-friendly and sustainable olefin production from a selective alcohol dehydration under mild conditions.

2. Experimental

2.1. Catalyst preparation

HPA/SiO_2 and ZnO/SiO_2 catalysts were prepared by incipient wetness impregnation of commercial SiO_2 (Grace G62, 99.7%, S_g = 230 m^2/g, V_P = 0.49 cm^3/g) with aqueous solutions of $H_3PW_{12}O_{40}$ (99%, Merck) and $ZnCl_2$ (99.5%, Aldrich), respectively. The impregnated precursors were dried at 373 K for 12 h and then calcined for 2 h in air at 573 K (HPA/SiO_2) or 623 K (ZnO/SiO_2). The HPA and ZnO loadings were 28 and 20%, respectively.

Al-MCM-41 sample was synthesized by the sol–gel method, according to Edler and White [29]. Sodium silicate solution (14% NaOH and 27% SiO_2, Aldrich), cetyltrimethylammonium bromide (Aldrich), aluminum isopropoxide (Aldrich), and deionizated water were used as the reagents. The composition of the synthesis gel was $7SiO_2$–xAl_2O_3–$2.7Na_2O$–3.7CTMABr–$1000H_2O$. The pH was adjusted to 10 using a 0.1 M H_2SO_4 solution, and then the gel was transferred to a Teflon-lined stainless-steel autoclave and heated to 373 K in an oven for 96 h. After crystallization, the solid was washed with deionizated water, dried at 373 K and finally calcined in air at 773 K.

Commercial Amberlyst 15 resin (Rohm and Haas, 37 m^2/g) was treated in N_2 at 373 K for 8 h before using in the catalytic tests. Amberlyst 15 is a well-known resin based on polystyrene, cross-linked with divinylbenzene (DVB) and sulfonated at a level equivalent to one sulfonic acid group per STY/DVB unit [30]. HY zeolite was obtained by triple ion exchange of a commercial NaY zeolite (UOP-Y54) with an 1 M aqueous solution of NH_4Cl at 353 K in a rotavapor during 2 h and subsequent calcination in air at 773 K. Commercial zeolites HZSM-5 (Zeocat Pentasil PZ-2/54, 0.43 wt.% Na), HMOR (Zeocat HZM-760), HBEA (Zeocat PB), SiO_2–Al_2O_3 (Ketjen LALPV) and γ-Al_2O_3 (Ketjen CK-300) samples were calcined in a dried air flow at 773 K before performing any characterization and catalytic tests.

2.2. Catalysts characterization

The crystalline structure of the calcined samples was verified by X-ray diffraction (XRD) using a Shimadzu XD-1 diffractometer and Ni-filtered Cu-Kα radiation (scan speed 2°/min). Textural properties of solid acids were measured by N_2 physisorption at 77 K in a Quantochrome Corporation NOVA-1000 sorptometer. Specific surface area (S_g) was determined by using the BET method. Pore volumes (V_P) and pore mean diameters (d_P) were estimated by applying Barret–Joyner–Halender (BJH) calculations. Zeolite micropore volumes were determined by the t-plot [31] method, using Harkins–Jura equation [32]. Elemental compositions were determined by atomic absorption spectroscopy (AAS).

The strength and density of surface acid sites were determined by temperature-programmed desorption (TPD) of NH_3 preadsorbed at 373 K. The previously calcined samples (200 mg) were treated in He (60 cm^3/min) at 773 K for 2 h, cooled down to 373 K, and then exposed to a NH_3(1%)/He stream for 45 min. Weakly adsorbed NH_3 was removed by flushing with He at 373 K during 2 h. Finally, the sample temperature was increased at 10 K/min and the NH_3 concentration in the effluent was measured by mass spectrometry (MS) in a Baltzers Omnistar unit.

The nature of surface acid sites was determined by Fourier transform infrared spectroscopy (FTIR) by using pyridine as a probe molecule and a Shimadzu FTIR-8101 M spectrophotometer. Sample wafers were formed by pressing 20–40 mg of the catalyst at 5 ton/cm^2 and transferred to a sample holder made of quartz. An inverted T-shaped Pyrex cell containing the sample pellet was used for the measurements. The previously calcined samples were initially outgassed at 723 K for 4 h and then a background spectrum was recorded after cooling the sample at room temperature. Data were obtained after admission of pyridine, adsorption at room temperature and evacuation at 423 K for 30 min. Spectra were always recorded at room temperature and the absorbance scale was normalized to 1-g samples.

The strength and density of surface basic sites were determined by temperature-programmed desorption (TPD) of CO_2 preadsorbed at 298 K. Samples (50 mg) were treated in air (60 cm^3/min) at the corresponding calcination temperature for 2 h, cooled down to room temperature, and then exposed to a 3% CO_2/N_2 stream for 15 min. Weakly adsorbed CO_2 was removed by flushing with N_2 at room temperature during 1 h. Afterwards, the sample temperature was increased at 10 K/min and the gas effluent was passed through a methanator at 673 K to convert CO_2 into CH_4. Concentration of CH_4 in the effluent was measured by gas chromatography using a flame ionization detector (FID).

Coke formed during reaction on the catalysts was determined by Temperature Programmed Oxidation (TPO). The used catalyst was separated by filtration from the reaction medium and dried overnight a 393 K. Afterwards, the TPO run was carried out passing an O_2(1%)/N_2 gas stream while heating from room temperature to 1000 K, at 10 K/min. The evolved carbon oxides were converted to CH_4 at 673 K over Ni(40%)/Kieselghur and monitored using a flame ionization detector (FID). Data acquisition was carried out by using Peak 356 software.

2.3. Catalytic tests

The liquid-phase dehydration of PHE was carried out at 363 K in a 600 ml autoclave (Parr 4843), using dehydrated cyclohexane (99%, Merck) as solvent. The autoclave was loaded under inert atmosphere with 150 ml of solvent and 0.5 g of catalyst previously calcined and then heated while stirring up to the reaction temperature. Then 3.0 ml of PHE (99%, Aldrich) were introduced to the reactor and the pressure was raised up to 2 bar in N_2 to start the reaction. Stirring speeds of 600 rpm and particle diameters lower than 100 μm (catalyst powder) were used to avoid mass transfer limitations.

The concentrations of unreacted PHE and products were followed during the reaction by ex situ gas chromatography using an Agilent 6850 chromatograph equipped with flame ionization detector and a 30 m Innowax capillary column with a 0.25 μm coating. Liquid samples were withdrawn from the reactor by using a loop under pressure in order to avoid flushing. The loop was designed to ensure that the total liquid volume withdrawn during the whole run was less than 5% of the initial reaction volume. The analysis was performed using n-dodecane (Sigma Aldrich, >99%) as an internal standard. Main reaction products were STY and AME, but three other minor chromatographic peaks were also detected, probably corresponding to dimers and oligomers, formed from STY [22,23], and other heavy compounds, formed from AME, that are named here as HP (heavy products). In order to perform carbon balance calculations, it was considered that these three compounds had the same carbon number and chromatographic response factors than AME, based on the proposed structure for these compounds given by other authors [23].

Conversion of PHE (X_{PHE}, mol of PHE reacted/mol of PHE fed) was calculated as $X_{PHE} = 100 \cdot (C^0_{PHE} - C_{PHE})/C^0_{PHE}$, where C^0_{PHE} is the initial PHE concentration and C_{PHE} is the PHE concentration at the reaction time t. Selectivities (S_j, mol of product j/mol of PHE reacted) at $t > 0$ were calculated as $S_j = C_j/\Sigma C_j$, where C_j is the concentration of product j in solution at the reaction time t. Yields (η_j, mol of product j/mol of PHE fed) were calculated as $\eta_j = 100 \cdot C_j/C^0_{PHE}$.

3. Results

3.1. Catalyst characterization

XRD was firstly performed in order to qualitatively determine the influence of calcination in dried air flow at 773 K on the zeolite crystalline structure. The XRD diffraction patterns obtained for calcined zeolites HBEA, HMOR, HY and HZSM-5 (Fig. 2) were similar to those reported in literature, indicating that zeolite crystalline structures were preserved after calcination. As well, the X-ray diffractogram of Al-MCM-41 is shown in Fig. 2. This XRD exhibited a strong diffraction peak at 2.2° arising from (1 0 0) reflection and two weaker peaks at 3.7° and 4.3° corresponding to (1 1 0) and (2 0 0) reflections, which are characteristic of the hexagonal arrangement of this mesoporous solid [29].

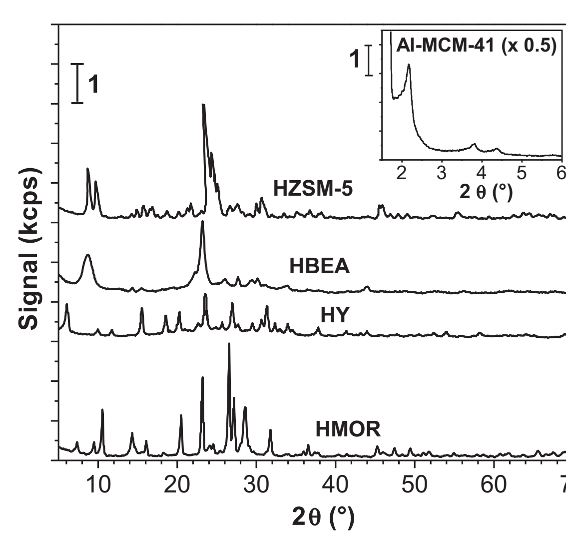

Fig. 2. XRD patterns for the calcined samples.

Table 1
Chemical composition and textural properties of the catalysts.

Catalyst	Si/Al[a]	S_g (m^2/g)[b]	V_P (cm^3/g)	d_P (Å)[d]	Channel dimensions (Å)
Amberlyst 15	–	37[c]	–	240[c]	
HPA/SiO_2	–	209	0.51[d]	180	
SiO_2–Al_2O_3	11.2	462	0.74[d]	59	
Al-MCM-41	20	925	0.68[d]	30	
ZnO/SiO_2	–	220	0.47[d]	170	
γ-Al_2O_3	0	180	0.25	41	
HBEA	12.5	560	0.17[e]		6.6 × 6.7; 5.6 × 5.6
HZSM-5	20	350	0.16[e]		5.1 × 5.5; 5.3 × 5.6
HY	2.4	660	0.26[e]		7.4
HMOR	60	610	0.28[e]		6.5 × 7.0; 3.4 × 4.8; 2.6 × 5.7

[a] Chemical composition determined by AAS.
[b] Specific surface area determined by the BET method.
[c] Proprietary information.
[d] Pore volume and diameter determined by the BJH method.
[e] Pore volume determined by the *t*-plot method.

The textural properties (specific surface area, pore volume, mean pore diameter) and Si/Al ratio of the calcined samples are shown in Table 1. The specific surface area of HPA/SiO_2 (209 m^2/g) and ZnO/SiO_2 (220 m^2/g) samples were similar than that of silica support (230 m^2/g). Mesoporous Al-MCM-41 exhibited the highest surface area (925 m^2/g), while SiO_2–Al_2O_3 showed an intermediate value (462 m^2/g). BET surface areas of zeolites HBEA (560 m^2/g) and HMOR (610 m^2/g) were higher than that determined for HZSM-5 (350 m^2/g). HY (660 m^2/g) showed a BET surface area some higher than HMOR but lower than the value of the starting NaY zeolite (700 m^2/g).

Acid density and relative acid strength of previously calcined samples were probed by TPD of NH_3 preadsorbed at 373 K. The obtained TPD curves are shown in Fig. 3. The amount of desorbed NH_3 was determined by deconvolution and integration of the TPD curves of Fig. 3 and it was taken as a measure of the acid site density, n_a. The resulting n_a values are reported in Table 2 in μmol/m^2 units.

ZnO/SiO_2 showed an intense and broad desorption band between 493 and 773 K with a maximum at 573 K, reflecting the presence of surface acid species that bind NH_3 with different strengths (Fig. 3a). Similarly, the NH_3 desorbed from SiO_2–Al_2O_3 gave rise to a peak at 483–493 K and a broad band at higher temperatures, also indicating the presence of surface sites of different acidity. In contrast, Al-MCM-41 did not exhibit the high-temperature NH_3 band but a single asymmetric broad band with a maximum around 482–496 K. For γ-Al_2O_3, only a small peak with a maximum at 473 K was observed, revealing that only weak acid sites are present on the surface of this oxide. The TPD curve of HPA/SiO_2 presented a broad desorption band in the range of 500–900 K with a peak at 846 K. On unsupported HPA, NH_3 desorbs in a single sharp peak at about 900 K [33] which accounts for the strong Brønsted acid sites present on this material. The broad strength distribution observed here for HPA/SiO_2 is probably the result of the HPA spreading on the silica surface that generates highly support interacting heteropolyacid species. The n_a values determined by integration of TPD curves in Fig. 3a are presented in Table 2. According to the literature [30], Amberlyst 15 contained the highest densities of surface acid sites (n_a = 126 μmol/m^2) among the samples, followed by ZnO/SiO_2 (n_a = 10.2 μmol/m^2). On an areal basis, the n_a values followed the order: Amberlyst 15 > ZnO/SiO_2 > SiO_2–Al_2O_3 > HPA/SiO_2 > Al-MCM-41 > γ-Al_2O_3.

The TPD curves obtained for HZSM-5, HY, HBEA and HMOR zeolites are presented in Fig. 3b. Consistently with previous work [27], the evolved NH_3 from mordenite HMOR gave rise to a low temperature peak between 400 and 550 K, assigned to weak acid sites, and a broad high temperature band (673–873 K) that reflects

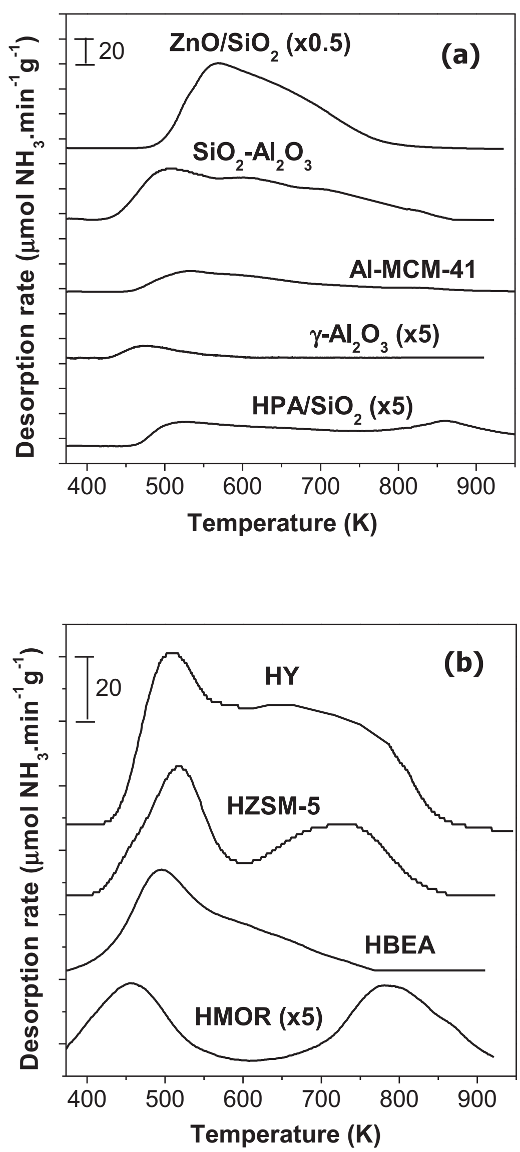

Fig. 3. TPD profiles of NH_3 [W_{CAT} = 200 mg; gas: NH_3(1%)/He; heating rate: 10 K/min]: (a) non-zeolitic solids and (b) zeolites.

Table 2
Acid–basic properties of the catalysts.

Catalyst	Acid site density (n_a)[a]		Basic site density (n_b)[b]		Acid site nature[c]	$n_b/(n_a+n_b)$	
	$T > 573$ K (μmol/m^2)	Total (μmol/m^2)	$T > 573$ K (μmol/m^2)	Total (μmol/m^2)	$L/(L+B)$	$T > 573$ K	Total
SiO_2	–	–	3.28×10^{-1}	3.95×10^{-1}	–	–	–
HPA/SiO_2	5.53×10^{-1}	7.83×10^{-1}	1.12×10^{-1}	1.51×10^{-1}	0.20	0.17	0.16
SiO_2–Al_2O_3	1.27	2.23	6.81×10^{-2}	8.49×10^{-2}	0.75	0.05	0.04
Al-MCM-41	1.57×10^{-1}	3.72×10^{-1}	1.85×10^{-2}	6.97×10^{-2}	0.81	0.11	0.16
ZnO/SiO_2	6.80	10.2	5.21×10^{-1}	6.19×10^{-1}	1.00	0.07	0.06
γ-Al_2O_3	1.12×10^{-2}	1.13×10^{-1}	6.14×10^{-2}	1.42×10^{-1}	1[d]	0.86	0.56
HBEA	3.04×10^{-1}	8.91×10^{-1}	3.82×10^{-2}	6.43×10^{-2}	0.55	0.11	0.07
HZSM-5	9.92×10^{-1}	2.20	1.02×10^{-2}	3.13×10^{-2}	0.50	0.01	0.01
HY	1.27	2.09	7.44×10^{-3}	3.92×10^{-2}	0.60	0.01	0.02
HMOR	1.14×10^{-1}	2.01×10^{-1}	$\cong 0$	1.46×10^{-2}	0.14	$\cong 0$	0.07

[a] Determined by TPD of NH_3.
[b] Determined by TPD of CO_2.
[c] Determined by FTIR of pyridine.
[d] From Ref. [39].

the presence of strong acid sites. The TPD curve corresponding to HBEA exhibited an asymmetric desorption band with a maximum at about 500 K, and is qualitatively similar to those reported for zeolites HBEA of similar Si/Al ratios [34]. The desorbed NH_3 profiles from HZSM-5 and HY are quite similar and showed a peak at about 520 K and a broad band between 583 and 773 K. On an areal basis, the n_a values showed that the surface acid sites density of the zeolites followed the order: HZSM-5 ≅ HY > HBEA > HMOR (Table 2).

The nature of surface acid sites was determined by FTIR of pyridine adsorbed on the previously calcined samples. The FTIR spectra (1400–1700 cm^{-1}) obtained after admission of pyridine, adsorption at room temperature and evacuation at 423 K are shown in Fig. 4. The pyridine adsorption bands at around 1540 cm^{-1} and between 1440 and 1460 cm^{-1} arise from pyridine adsorbed on Brønsted (B) and Lewis (L) sites, respectively [35–38]. The relative contributions of Lewis and Brønsted acid sites were obtained by deconvolution and integration of pyridine absorption bands at around 1450 and 1540 cm^{-1} in Fig. 4 and the results are summarized in Table 2.

The FTIR spectrum of ZnO/SiO_2 in Fig. 4a exhibited only two overlapping absorption bands due to pyridine adsorbed on Lewis acid sites. Similarly, in a previous paper, the characterization by FTIR of adsorbed pyridine on commercial γ-Al_2O_3 showed that this material contains only Lewis acid sites [39]. Instead, both Lewis and Brønsted acid sites are present on Al-MCM-41 and SiO_2–Al_2O_3 surface. The coordinately bound pyridine band appears at 1455 cm^{-1} reflecting the adsorption of pyridine on Lewis acid sites associated with tricoordinate Al atoms [40]. The band at 1543–1545 cm^{-1} reveals the adsorption of pyridine on Brønsted acid sites. On the other hand, the areal peak relationship between Lewis and total sites, $L/(L+B)$, was slightly higher on Al-MCM-41 ($L/(L+B) = 0.81$) than on SiO_2–Al_2O_3 ($L/(L+B) = 0.75$). The HPA/SiO_2 sample also showed two pyridine absorption peaks at 1451 and 1539 cm^{-1}, indicating the presence of both Lewis and Brønsted surface sites (Fig. 4a). However, The $L/(L+B)$ ratio obtained for HPA/SiO_2 was 0.20, which is rather lower than in the case of SiO_2–Al_2O_3 and Al-MCM-41 (Table 2). The fact that HPA/SiO_2 displayed IR bands due to both Brønsted and Lewis acid sites suggests that, upon impregnation of HPA on SiO_2, the Keggin structure, that accounts for the Brønsted acid species, partially transforms giving rise to lacunary or unsaturated species of Lewis acid character formed by interaction with the silica support [41,42]. Sample Amberlyst 15 was not characterized by FTIR of adsorbed pyridine because of its low thermal stability. However, it is well known that this sulfonic resin contains only Brønsted acidity, ascribed to the presence of sulfonic groups (–SO_3H) [43,44]. Thus, the $L/(L+B)$ ratio of Amberlyst 15 was assumed to be equal to 0 (Table 2). In summary, the $L/(L+B)$ ratio followed the pattern: ZnO/SiO_2 ≅ γ-Al_2O_3 > Al-MCM-41 > SiO_2–Al_2O_3 > HPA/SiO_2 > Amberlyst 15.

Fig. 4b shows the IR spectra obtained on zeolites HY, HBEA, HZSM-5 and HMOR. On HY, the pyridine absorption bands associated with Brønsted and Lewis acid sites appeared at 1542 and

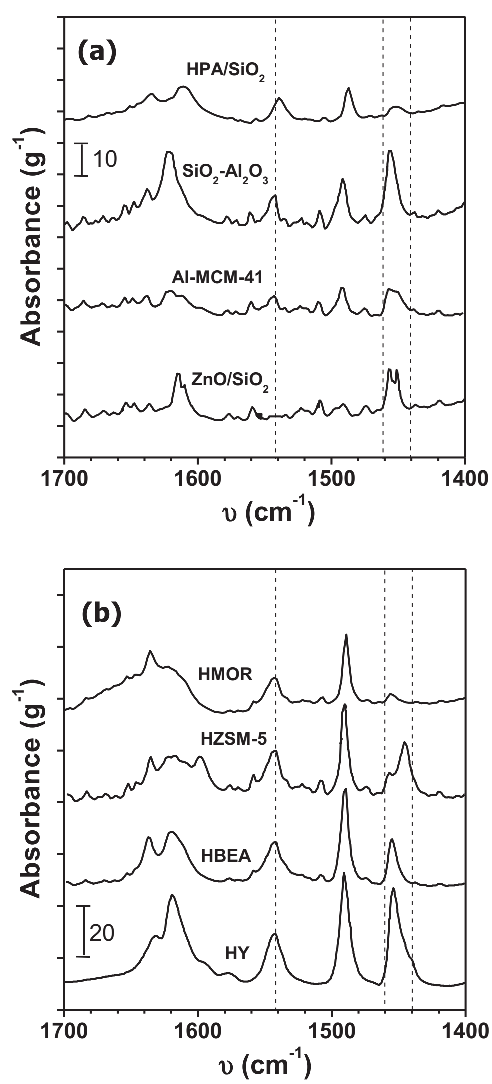

Fig. 4. FTIR spectra of pyridine adsorbed at 298 K and evacuated at 423 K for 0.5 h: (a) non-zeolitic solids and (b) zeolites.

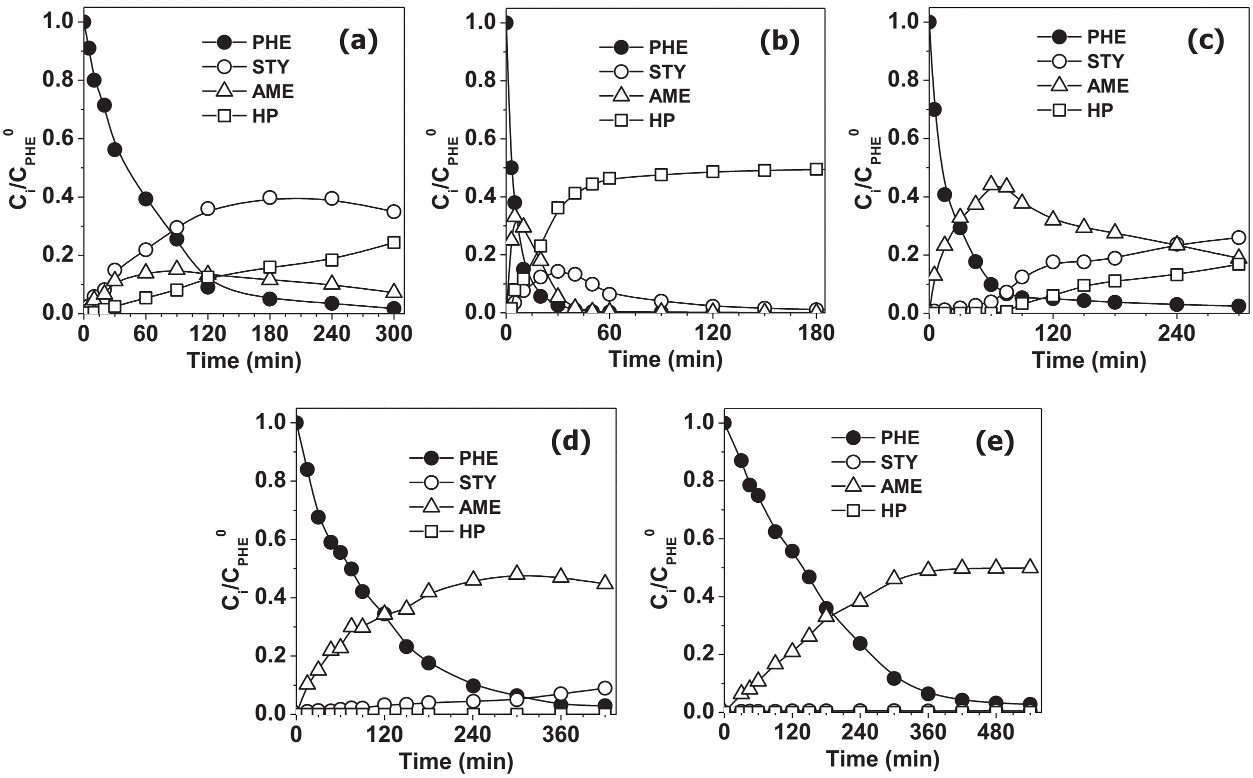

Fig. 5. Product and reactant dimensionless concentration profiles as a function of time for non-zeolitic samples: (a) Amberlyst 15; (b) HPA/SiO_2; (c) SiO_2–Al_2O_3; (d) Al-MCM-41; and (e) ZnO/SiO_2 [T = 363 K, W_{CAT} = 0.5 g, PHE/cyclohexane = 3:150 (ml), stirring rate = 600 rpm].

1454 cm^{-1}, respectively. These two bands were present even after evacuation at 723 K (spectra not shown here), indicating that zeolite HY contains strong Brønsted and Lewis acid sites, in agreement with TPD of NH_3 (Fig. 3b). The $L/(L+B)$ ratio for HY was 0.60 (Table 2). On HBEA, the IR bands due to pyridine adsorbed on Brønsted and Lewis acid sites appeared at 1542 and 1455 cm^{-1}, respectively. The $L/(L+B)$ ratio obtained for HBEA was 0.55 (Table 2). On HZSM-5, it is observed that the 1440–1460 cm^{-1} band was split in two overlapping peaks corresponding to pyridine adsorbed on Al (1450 cm^{-1}) and Na (1445 cm^{-1}) Lewis acid sites [45]. An infrared band at 1542 cm^{-1}, due to pyridine adsorbed on Brønsted acid sites, was also observed. The concentration of Brønsted and Lewis acid sites was the same on HZSM-5 surface ($L/(L+B)$ = 0.5, Table 2). Zeolite HMOR showed both Lewis and Brønsted pyridine adsorption bands at 1453 and 1544 cm^{-1}, respectively. From the integration of these bands, a $L/(L+B)$ ratio equal to 0.14 was obtained (Table 2). Thus, the $L/(L+B)$ ratio for the four zeolites followed the order: HY ≅ HBEA ≅ HZSM-5 > HMOR.

Basic properties were probed by TPD of CO_2 preadsorbed at room temperature on the previously calcined samples. The total amount of desorbed CO_2 was determined by numerical integration of the TPD profiles. The values thus obtained were taken as an indication of the basic site density, n_b. Besides, the amount of CO_2 desorbed at temperature higher than 573 K was discriminated, as an indication of the density of strong basic site. The resulting values are reported in Table 2 in μmol/m^2 units. It was observed that, for all the samples except γ-Al_2O_3, the total amount of desorbed CO_2 was between one and two orders of magnitude lower than the amount of desorbed NH_3. The ratio $n_b/(n_a+n_b)$ is also given in Table 2 as an indicator of the basic/acid balance in the samples. It is very clear from these values that both the strong basic site density (T > 573 K) and the total basic site density are much lower than the corresponding acid site density; in general the $n_b/(n_a+n_b)$ ratio was lower than 0.17. Even more, the $n_b/(n_a+n_b)$ ratio was lower or equal than 0.1 in the case of zeolites. Only in the case of γ-Al_2O_3 the total basic site density was similar to the total acid site density.

In summary, catalyst characterization results showed that the density, nature and strength of surface acid sites are very different when comparing the catalysts used in this work. On the other hand, in all of the cases excepting γ-Al_2O_3, the concentration of basic sites was considerably lower than the acid site density. Thus, the results showed in general a clear acidic character of the samples used in this work.

3.2. *Catalytic tests*

The evolution of the reactant and product concentrations as a function of reaction time for all the catalysts used in this work, excepting γ-Al_2O_3, are presented in Fig. 5 (non-zeolitic samples) and Fig. 6 (zeolites). Amberlyst 15 formed initially STY and AME at similar rates (Fig. 5a) and then both products were progressively converted to HP, in agreement with the reaction network depicted in Fig. 1. The initial AME formation rate on HPA/SiO_2 was clearly higher compared to that of STY; then, both primary products were rapidly transformed into HP (Fig. 5b). Over SiO_2–Al_2O_3 (Fig. 5c), PHE was essentially converted to AME via an intermolecular dehydration mechanism; then AME was transformed into STY and HP following the reaction pathways (3) and (5) of Fig. 1, respectively. Similarly to SiO_2–Al_2O_3 sample, Al-MCM-41 produced initially almost exclusively AME that was slowly converted to STY (Fig. 5d); however, Al-MCM-41 did not convert AME to HP. Finally, the ZnO/SiO_2 sample produced selectively AME during the 9-h catalytic test (Fig. 5e), reaching the maximum theoretical AME yield that corresponds to the stoichiometry of the intermolecular dehydration.

Regarding the catalytic results obtained on zeolites, Fig. 6a shows that zeolite HBEA converted PHE essentially to STY, but STY reached a maximum concentration since it was then converted

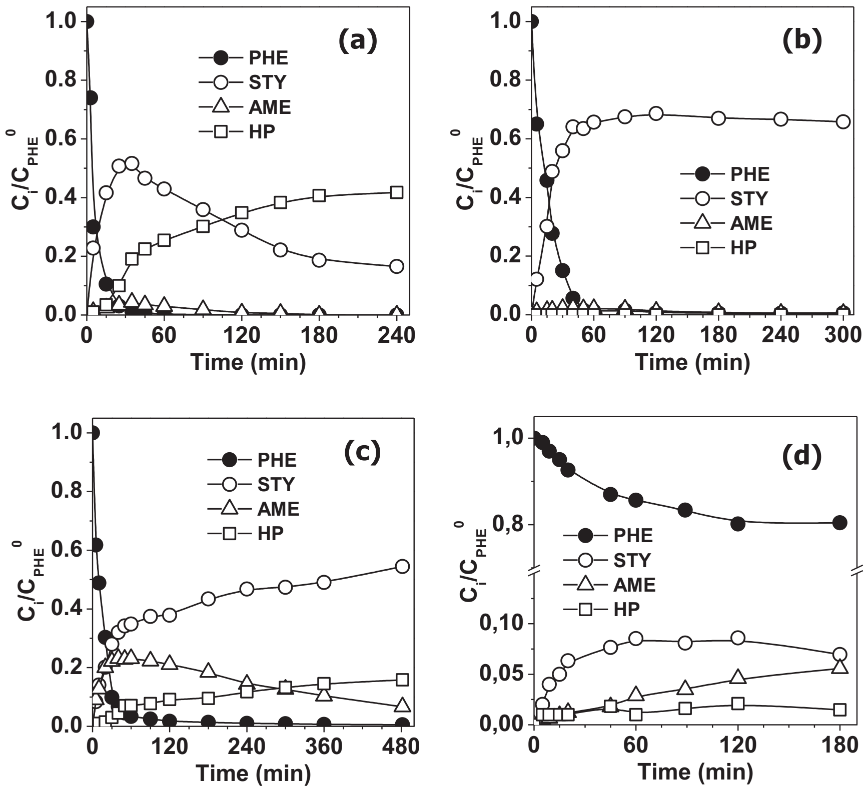

Fig. 6. Product and reactant dimensionless concentration profiles as a function of time for zeolites: (a) HBEA; (b) HZSM-5; (c) HMOR; and (d) HY [T = 363 K, W_{CAT} = 0.5 g, PHE/cyclohexane = 3:150 (ml), stirring rate = 600 rpm].

to HP through secondary reactions. Instead, zeolite HZSM-5 was highly selective to the formation of STY during the whole run (Fig. 6b). Zeolite HMOR formed initially AME and STY at similar rates but then AME was slowly converted to STY and HP (Fig. 6c). Similarly to HBEA, HY converted selectively PHE into STY but only 20% PHE conversion was reached in about 2 h and then no further conversion was observed with time, indicating a rapid deactivation (Fig. 6d) as it was suggested in a previous work [46].

In order to obtain quantitative data for comparing the catalysts activity and selectivity, the initial PHE conversion rates (r^0_{PHE}) were determined from the curves of Figs. 5 and 6 by applying numerical polynomial fitting and subsequent differentiation of the obtained polynomial at zero time. The initial selectivity (t = 0) to STY was calculated as $S^0_{STY} = r^0_{STY}/(r^0_{STY} + 2 \cdot r^0_{AME})$. The values obtained for S^0_{STY} (%) and for r^0_{PHE} per gram of catalyst (mol/min g) and per μmol of adsorbed NH_3 (mol/min μmol NH_3) are shown in Table 3. The styrene selectivity (S_{STY}) and carbon balance obtained at 90% conversion of PHE were also included in Table 3. It is observed that HPA/SiO_2, SiO_2–Al_2O_3, Al-MCM-41 and ZnO/SiO_2 are not selective for the formation of styrene; the S^0_{STY} and S_{STY} values were in fact lower than 11% in all the cases. Amberlyst 15 promoted better the styrene selectivity (S^0_{STY} = 35.6%) but exhibited low activity for converting PHE; for example, the r^0_{PHE} value per gram of catalyst was one order of magnitude lower on Amberlyst 15 than on HPA/SiO_2 (Table 3). The highest initial selectivities to styrene were obtained on zeolites HBEA (S^0_{STY} = 96.4%) and HZSM-5 (S^0_{STY} = 94.2%), but HBEA was more active than HZSM-5. However, the selectivity to styrene decreased with the progress of the reaction on HBEA (S_{STY} = 77.5%) while remained practically constant on HZSM-5 (S_{STY} = 92.6%). HY gave a high initial selectivity to STY (S^0_{STY} = 82.7%), but it was less active than HBEA and HZSM-5, probably because it deactivated from the very beginning of the reaction.

Table 3
Catalytic results in the liquid phase dehydration of 1-phyenylethanol [T = 363 K, W_{CAT} = 0.5 g, PHE/cyclohexane = 3:150 (ml)].

Catalyst	r^0_{PHE} [a]		S^0_{STY} [b] (%)	S_{STY} [c] (%)	Carbon balance[d] (%)
	(mol/min g) × 10^3	(mol/min μmol NH_3) × 10^3			
Amberlyst 15	0.71	0.15	35.6	40.9	98.3
HPA/SiO_2	6.56	40.20	10.0	10.9	98.5
SiO_2–Al_2O_3	2.46	2.96	2.5	4.5	99.8
Al-MCM-41	0.67	1.95	2.5	4.9	100
ZnO/SiO_2	0.19	0.08	0	0	99.8
HBEA	3.04	6.09	96.4	77.5	63.8
HZSM-5	1.90	2.47	94.2	92.6	75.3
HY	0.29	0.21	82.7	–	–
HMOR	2.38	19.50	29.1	35.4	88.4

[a] Initial PHE conversion rate.
[b] Initial selectivity to STY.
[c] Selectivity to STY at X_{PHE} = 90%.
[d] Carbon balance at X_{PHE} = 90%.

Zeolite HMOR was clearly less selective to the initial formation of styrene ($S^0_{STY} = 29.1\%$) than HBEA or HZSM-5, but exhibited higher activity per acid site ($r^0_{PHE} = 19.50$ mol/min µmol NH_3). Finally, data in Table 3 show that the carbon balance was close to 100% on non-zeolitic samples but decreased significantly on zeolites, probably reflecting a strong adsorption of reactant and product molecules on the zeolite surface followed by formation of coke precursors. In fact, it has been reported that the strong adsorption of STY on zeolites leads to formation of dimers and oligomers [22,23]. Similarly, PHE adsorption can produce AME. All of these compounds can be formed in the micropores of HBEA and HMOR or in the channel intersections of HZSM-5, but they cannot easily diffuse throughout the zeolite micropores [47]. Thus, large amounts of HP can be retained inside microporous structure and form coke precursors, thereby explaining the carbon unbalance observed in Table 3 for zeolite samples. The TPO profile obtained for used HZSM-5 sample (Fig. 10) is consistent with this assumption. At least two types of carbonaceous compounds were burnt in the TPO experiment: (a) the first one between 473 and 673 K, with a maximum at 533 K; (b) the second one between 673 and 973 K, in agreement with results found in previous works [48]. The total carbon content was about 12.3 wt.%, indicating that a large amount of carbon compounds was retained inside the zeolite microporous structure. To obtain more insight on the effect of coke formation on catalyst deactivation two consecutive catalytic tests were performed on zeolite HZSM-5. The procedure was as follows: immediately after PHE was completely converted in the first test, the same amount of initial moles of PHE was introduced to the reactor (without opening it) and a second consecutive test was carried out. It was found that the initial PHE conversion rate dropped from 1.9×10^{-3} mol/min g (first test) to 1.3×10^{-3} mol/min g (second test). Consistently, complete PHE conversion in the first and second runs was achieved in 60 min and 90 min, respectively. However, the maximum yield in STY was almost the same with both fresh and used catalyst.

It is worth noticing that among the non-zeolitic samples, γ-Al_2O_3 showed no catalytic activity in the liquid-phase dehydration of PHE in these experimental conditions. This catalyst is one of the most traditionally used to perform gas phase alcohol dehydrations at temperatures higher than 473 K [2–4]. However, the weak Lewis acid sites in γ-Al_2O_3, strong enough to dehydrate alcohols in gas phase at high temperature, are too weak to perform the same task in liquid-phase, showing that the acid requirements change significantly, when we change from gas phase ($T > 473$ K) to liquid phase ($T \leq 373$ K).

4. Discussion

The most important factors that influence the selectivity during an alcohol dehydration reaction are acid and textural properties of the catalyst. Among them, density, strength and nature of the acid sites are very important. However, textural properties of the catalyst might also strongly influence the selectivity in the case of microporous solids [49].

In order to analyze the influence of the nature of the catalyst acid sites on the STY selectivity, the results were arranged according to the $L/(L+B)$ ratio as variable to assess the catalysts. The initial selectivity to STY, S^0_{STY}, and the selectivity at maximum yield in STY, $S_{STY}(\eta^{max}_{STY})$, were represented against the $L/(L+B)$ ratio for the active catalysts and the results are shown in Fig. 7a and b, respectively. In both figures it is possible to identify three different catalyst categories according to the values of $L/(L+B)$ ratio and selectivity to STY: (1) catalysts with $L/(L+B) \geq 0.75$, showing low initial selectivity to STY; (2) catalysts with $L/(L+B) \leq 0.20$, showing medium initial selectivity to STY; and (3) catalysts with $L/(L+B) \cong 0.5$–0.6, showing high initial selectivity to STY.

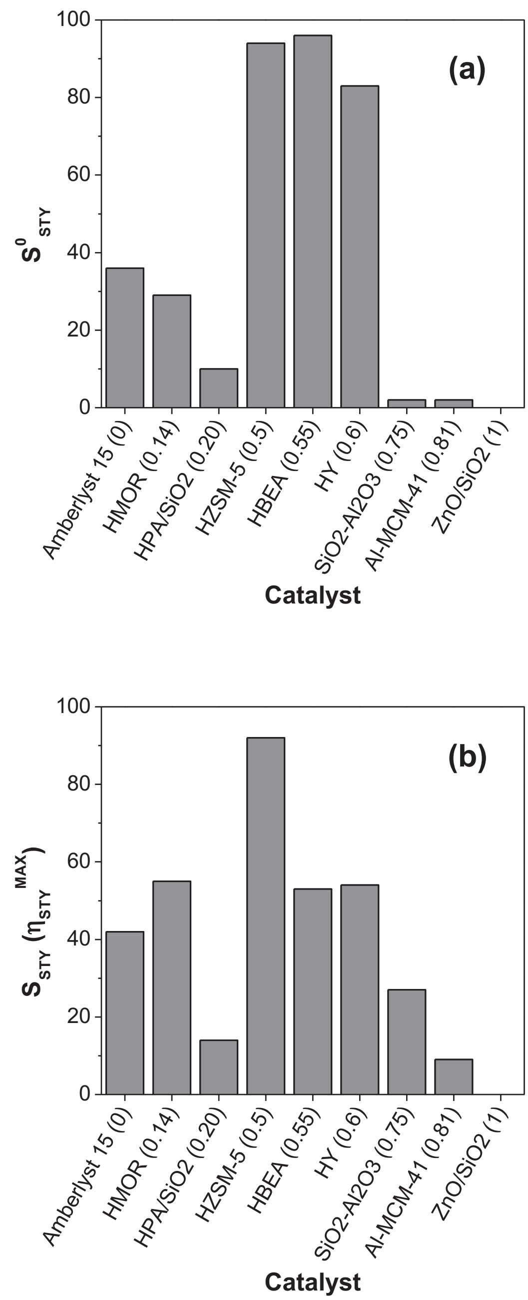

Fig. 7. STY selectivity as a function of $L/(L+B)$ ratio: (a) initial STY selectivity and (b) STY selectivity at maximum yield.

It is well accepted that the adsorption of an alcohol over either Lewis or Brønsted acid sites (identified with A in Fig. 8) may be schematically represented as in Fig. 8a [1,50]. Thus, this scheme counts for the two alternatives depending on the nature of acid site A: (1) PHE adsorbs on a Lewis acid site through the interaction between the oxygen atom of the –OH functional group and the electron-deficient Lewis site and (2) PHE interacts through the oxygen atom of the –OH functional group with the proton of the Brønsted site [1].

In the case of catalysts containing not only acid but also basic sites, the generally accepted alcohol adsorption mode is the one shown in Fig. 8b [51–53]. In this case, the alcohol adsorption can take place through the simultaneous interactions of the oxygen atom of the –OH functional group with the acid (A) site and one hydrogen atom of the $-CH_3$ group with the basic (B) surface site. In

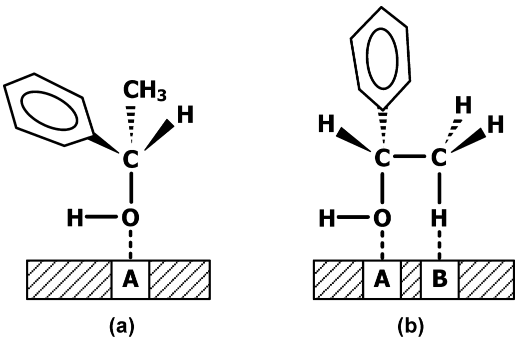

Fig. 8. Proposed 1-phenylethanol adsorption mode over: (a) acid sites and (b) acid and basic sites [A: acid site; B: basic site].

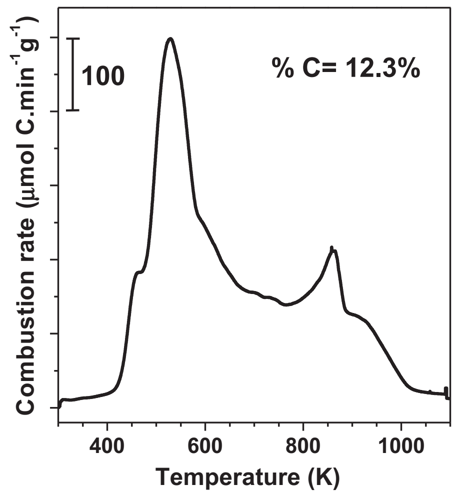

Fig. 10. TPO profile [W_{CAT} = 12 mg; gas: O_2(1%)/N_2; heating rate: 10 K/min] for the used HZSM-5 catalyst after liquid-phase dehydration of 1-phenylethanol at 363 K.

principle, this will be the main adsorption mode only if the surface concentration of acid and basic sites is approximately the same. However, for all of the samples used in this work, TPD of CO_2 showed that the surface basic site density was between one and two orders of magnitude lower than the surface acid site density (Table 2). Then, it is likely that the adsorption mode represented in Fig. 8b is not significant for the analysis that follows, due to the low possibility of finding neighboring basic and acid sites.

The initial STY selectivity over the catalysts with $L/(L+B) \geq 0.75$ (Fig. 7a) was practically null, which can be explained considering the PHE selective adsorption on Lewis sites, as described in Fig. 8a. Then, AME is formed by nucleophilic attack to the electron-deficient C atom of this surface species by either a PHE molecule in liquid phase, through an Eley-Rideal mechanism (Fig. 9a), or a PHE molecule adsorbed on a neighbor site [27]. As a consequence, AME was the main primary product when solid acids with $L/(L+B) \geq 0.75$ were used as catalysts. Even more, if the catalyst contains exclusively weak Lewis acid sites, such as γ-Al_2O_3, PHE is not activated properly and the solid shows no catalytic activity at the experimental conditions used in this work.

On the other hand, when the catalysts have mainly Brønsted acid sites ($L/(L+B) \leq 0.20$), both the intermolecular and intramolecular dehydration take place and thus AME and STY are initially obtained (Fig. 7a, Tables 2 and 3). The formation of AME can occur in a similar way to that described above. However, catalysts containing mainly surface Brønsted acid sites and very low basic site concentration produce also STY as primary product. In this case, both the simultaneous formation of the good leaving group H_2O^+ and the abstraction of a hydrogen atom from the methyl group are necessary to produce STY. The hydrogen abstraction from the –CH_3 group of PHE adsorbed on Brønsted sites has been proposed in previous works assuming the formation of a six-membered ring intermediate [27,28]. This mechanism explains: (1) the formation of the H_2O^+ leaving group; (2) the abstraction of a hydrogen atom from the methyl group; and (3) the regeneration of the catalytic site. Similar surface intermediates have been previously proposed for the dehydration of other alcohols over solid acids [1,50].

Finally, initial selectivities to STY higher than 80% (Fig. 7a) were obtained when the catalysts have a similar surface density of Lewis and Brønsted acid sites ($0.5 \leq L/(L+B) \leq 0.6$). In this case, there is a large probability of finding neighboring Lewis and Brønsted sites. Then, the adsorption of PHE can take place

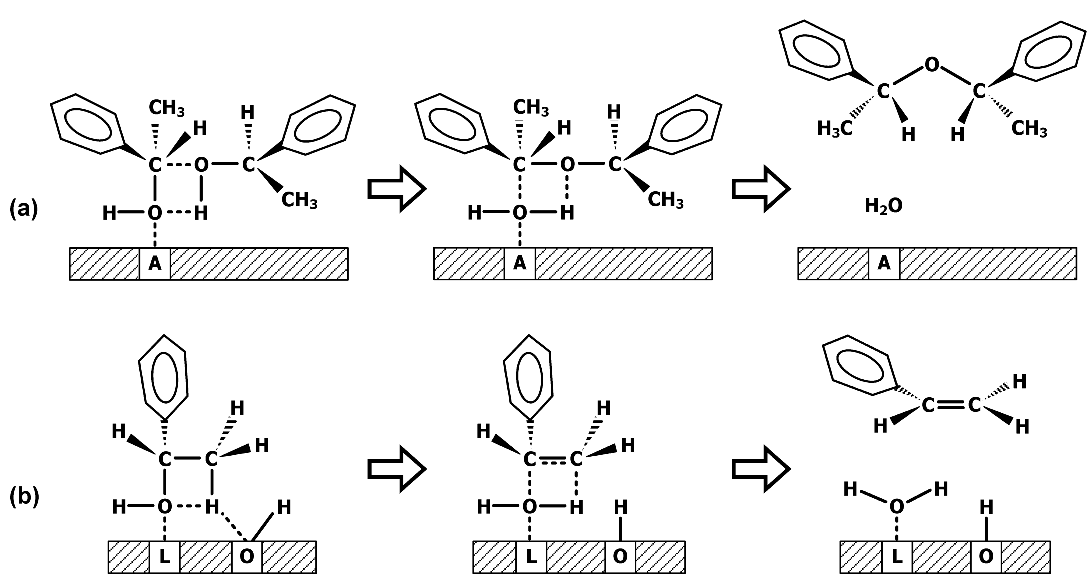

Fig. 9. Proposed mechanisms for: (a) intermolecular 1-phenylethanol dehydration into α-methylbenzyl ether on surface acid sites and (b) intramolecular 1-phenylethanol dehydration into styrene over a catalytic surface with similar density of Lewis and Brønsted acid sites.

through the simultaneous interaction of: (1) the oxygen atom of the –OH functional group with a Lewis acid site and (2) one hydrogen atom of the methyl group with the oxygen of a neighboring Brønsted site (Fig. 9b). Hence, both the formation of the H_2O^+ leaving group and the abstraction of a hydrogen atom from the $-CH_3$ group are possible. The probability to form this surface intermediate when $0.5 \leq L/(L+B) \leq 0.6$ would be higher than when $L/(L+B) \leq 0.20$. Therefore the intramolecular dehydration is promoted when the Lewis and Brønsted site density on the catalyst surface is similar, boosting the initial selectivity to STY. Water evolved in this reaction can be either desorbed or remain adsorbed, depending on the strength of the Lewis acid site. If it remains adsorbed, this water molecule modifies the solid acid surface producing a new strong Brønsted site. In this last case, the new mechanism on the modified surface will become the one previously proposed for PHE dehydration during a long catalytic test [28].

It is worth noticing that HY zeolite, with $L/(L+B) = 0.6$ and high concentration of strong surface acid sites (Table 2 and Fig. 3), showed an initial selectivity to STY of about 84% (Fig. 7a). However, the evolution of the PHE conversion as a function of time showed that an important deactivation takes place on this catalyst. HY zeolite presents a faujasite structure with a three-dimensional channels network and a pore diameter of 7.4 Å (12 members ring) [54]. These channels intersect each other forming cages with an inside diameter of 13 Å, which contains the strongest Brønsted acid sites. Then, it is highly probable that large amounts of HP are formed inside the HY cages, becoming larger than the pores. These HP compounds will remain inside cages, blocking the channels structure and the strongest acid sites, as it was proposed in a previous work [46]. Then, PHE interacted preferentially with the weak acid sites present on the external surface and it was slowly converted into AME. As a consequence, the selectivity to STY diminished during run from 84 to 55% (Fig. 7b).

HBEA zeolite ($L/(L+B) = 0.55$) was the most active zeolite in the PHE dehydration with an initial selectivity to STY equal to 96% (Fig. 7a). However, selectivity to STY decayed with time to reach 53% at maximum yield in STY (Fig. 7b) due to an important HP formation from STY (Fig. 6a). This molecular sieve has a three-dimensional porous network of 6.6×6.7 Å and 5.6×5.6 Å, formed by 12 member ring [54]. In this case, the pore size is large enough to allow the formation of HP from STY and their diffusion outside the micropores, diminishing thus the selectivity to STY.

Although the acid properties of HBEA and HZSM-5 are quite similar regarding the nature and strength of the acid sites, the product distribution observed over these samples after a period of time were rather different (Figs. 6 and 7). The more likely explanation for this fact can be found in the different microporous structure of HBEA and HZSM-5 zeolites. HZSM-5 has a three-dimensional porous network of medium pore size (5.1×5.5 Å and 5.3×5.6 Å) formed by 10 members ring [54], big enough to accommodate only some monoaromatic compounds. As a consequence, in contrast with HBEA, HZSM-5 structure avoids the formation of bulky reaction intermediates inside the channels to produce HP from STY [55]. In this way, the selectivity to STY was kept at 92% during the whole experiment (Fig. 7b).

In summary, from the previous analysis we can say that, catalysts with strong acid sites and a similar density of Lewis and Brønsted sites (HZSM-5, HBEA, HY) show the highest initial selectivity to STY, whereas AME is preferentially formed on the solid acids having mainly surface Lewis acid sites (SiO_2–Al_2O_3, Al-MCM-41, ZnO/SiO_2) or Brønsted acid sites (Amberlyst 15, HMOR, HPA/SiO_2). However, high selectivity to STY, i.e. higher or equal to 90%, at total PHE conversion was only achieved over HZSM-5, which has the most appropriate microporous structure. Thus, shape selectivity plays a very important role avoiding AME and HP formation.

5. Conclusions

The influence of the nature and strength of surface acid sites and that of the porous structure on the liquid-phase 1-phenylethanol dehydration were determined by performing a systematic and exhaustive study that covered a wide range of micro and mesoporous solid acid catalysts and different characterization techniques.

It was found out that the initial selectivity of the solid acid catalysts in the liquid-phase 1-phenylethanol dehydration strongly depends on the surface Brønsted to Lewis ratio. On this basis, three different categories of solid acid catalysts are proposed: (1) with major proportion of surface Brønsted acid sites; (2) with major proportion of Lewis acid sites; and (3) with comparable proportions of surface Brønsted and Lewis acid sites.

Catalysts having mainly surface Brønsted acid sites give alpha-methylbenzyl ether as major product of 1-phenylethanol dehydration and styrene in minor grade. If the acid sites are strong enough, these primary products are converted at high rate into heavy products.

When the catalysts have mainly surface Lewis acid sites of medium-high strength, 1-phenylethanol is selectively dehydrated into alpha-methylbenzyl ether through an intermolecular dehydration. This type of dehydration is favored by the preferential interaction of oxygen atom of the –OH group of 1-phenylethanol with the Lewis acid site. The ether thus formed is consecutively converted into styrene and heavy products. The formation of both styrene and heavy products from the ether increases as the surface Brønsted acid sites proportion raises.

High initial selectivity to styrene is only achieved when the catalysts have similar surface concentrations of Lewis and Brønsted acid sites. This is suggesting that when 1-phenylethanol is interacting simultaneously with Lewis and Brønsted sites, the intramolecular dehydration to styrene is favored by the formation of a surface cyclic intermediate. However, this high initial selectivity to the olefin is maintained during the run only if a medium pore size zeolite, as HZSM-5, is employed as catalysts. Pore sizes larger than the one of HZSM-5 allow the formation of surface bulky intermediates to produce heavy products. These heavy products can diffuse through the porous structure diminishing thus the selectivity to the desired product. Then, shape selectivity plays a key role in the selective liquid-phase dehydration of 1-phenylethanol into styrene.

These concluding remarks could be of importance for the design of heterogeneous catalytic process to be employed in the dehydration of 1-phenylethanol and other alcohols with similar structure, avoiding thus expensive and difficult separation processes and the negative environmental impact associated with homogeneous catalysis.

Acknowledgements

We thank the Universidad Nacional del Litoral (UNL), Consejo Nacional de Investigaciones Científicas y Técnicas (CONICET) and Agencia Nacional de Promoción Científica y Tecnológica (ANPCyT), Argentina, for the financial support to this project.

References

[1] E. Ortiz-Islas, T. López, J. Navarrete, X. Bokhimi, R. Gómez, J. Mol. Catal. A: Chem. 228 (2005) 345–350.
[2] C.N. Winnick, U.S. Patent 4,207,424 (1980), Halcon Research & Development Corporation.
[3] G.P. Babu, R.S. Murthy, V. Krishnan, J. Catal. 166 (1997) 111–114.
[4] N.P. Makgoba, T.M. Sakuneka, J.G. Kootzen, C. Van Schalkwyk, J.M. Botha, C.P. Nicolaides, Appl. Catal. A: Gen. 297 (2006) 145–150.
[5] T. Takahashi, T. Kai, Can. J. Chem. Eng. 66 (1988) 433–437.
[6] J. Longe, C.M.A.M. Mesters, Appl. Catal. A: Gen. 210 (2001) 247–255.

[7] S.K. Jana, H. Takahashi, M. Nakamura, M. Kaneko, R. Nishida, H. Shimizu, T. Kugita, S. Namba, Appl. Catal. A: Gen. 245 (2003) 33–41.
[8] W.S. Dubner, L.M. Candela, U.S. Patent 5639928 (1997), ARCO Chemical Technology, L.P.
[9] P. Vázquez, L. Pizzio, C. Cáceres, M. Blanco, H. Thomas, E. Alesso, L. Finkielsztein, B. Lantaño, G. Moltrasio, J. Aguirre, J. Mol. Catal. A: Chem. 161 (2000) 223–232.
[10] E.C. Wijnbelt, E.H. Hekelaar, U.S. Patent 2010/0,240,939 A1 (2010).
[11] H.-U. Blaser, M. Studer, Appl. Catal. A: Gen. 189 (1999) 191–204.
[12] W.F. Hoelderich, Catal. Today 62 (2000) 115–130.
[13] K. Weissermel, H.J. Arpe, Industrial Organic Chemistry, 4th edition, Wiley-VCH, 2003.
[14] Ullmann's Encyclopedia of Industrial Chemistry, Wiley-VCH Verlag GmbH & Co. KgaA, 2002.
[15] R. Pamukcu, G.A. Piazza, P. Gross, G. Sperl, K. Brendel, U.S. Patent 5,965,619 (1999), Cell Pathways Inc.
[16] M.M. Chartrain, N.C. Connors, G.M. Garrity, R.C. Olewinski Jr., T.R. Verhoeven, J. Zhang, U.S. Patent 5,605,819 (1997), Merck.
[17] I.E. Nifant'ev, Y.A. Dubitsky, A.A. Sitnikov, U.S. Patent 6,271,411 (2001), Montell Technology Company.
[18] H. Müller, P. Trubenbach, B. Rieger, J.M. Wagner, U. Dietrich, U.S. Patent 6,087,536 (2000), Basf.
[19] M. Becker, S. Khoobiar, U.S. Patent 3,526,674 (1970), Halcon International Inc.
[20] H. Dirkzwager, M. van Zwienen, WO Patent 99/58480 (1999), Shell Int. Res.
[21] Y. Konai, M. Hino, H. Enari, K. Yoshida, GB Patent 2,176,801 (1987), Kureha Kagaku Kogyo Kabushiki Kaisha.
[22] J. Lange, V. Otten, J. Catal. 238 (2006) 6–12.
[23] J. Lange, V. Otten, Ind. Eng. Chem. Res. 46 (2007) 6899–6903.
[24] N.A. Khan, J.-S. Hwang, S.H. Jhung, Bull. Korean Chem. Soc. 32 (2011) 1327–1330.
[25] J.P. Pérez Valencia, E.S.N. Sayans, Ind. Eng. Chem. Res. 50 (2011) 5485–5489.
[26] A. Tarlani, A. Riahi, M. Abedini, M.M. Amini, J. Muzart, J. Mol. Catal. A: Chem. 260 (2006) 187–189.
[27] N.M. Bertero, C.R. Apesteguía, A.J. Marchi, Catal. Commun. 10 (2008) 261–265.
[28] N.M. Bertero, C.R. Apesteguía, A.J. Marchi, Catal. Commun. 10 (2009) 1339–1344.
[29] K.J. Edler, J.W. White, Chem. Mater. 9 (1997) 1226–1233.
[30] P.F. Siril, H.E. Cross, D.R. Brown, J. Mol. Catal. A: Chem. 279 (2008) 63–68.
[31] B.C. Lippens, B.G. Linsen, J.H. De Boer, J. Catal. 3 (1964) 32–37.
[32] W.D. Harkins, G. Jura, J. Chem. Phys. 11 (1943) 431–432.
[33] V.K. Díez, B.J. Marcos, C.R. Apesteguía, J.I. Di Cosimo, Appl. Catal. A: Gen. 358 (2009) 95–102.
[34] Y. Miyamoto, N. Katada, M. Niwa, Microporous Mesoporous Mater. 40 (2000) 271–281.
[35] E.P. Parry, J. Catal. 2 (1963) 371–379.
[36] J.W. Ward, J. Catal. 10 (1968) 34–46.
[37] H. Knözinger, Adv. Catal. 25 (1976) 184–271.
[38] G. Busca, Catal. Today 41 (1998) 191–206.
[39] M.S. Avila, Ch.I. Vignatti, C.R. Apesteguía, V. Venkat Rao, K. Chary, T.F. Garetto, Catal. Lett. 134 (2010) 118–123.
[40] J. Wang, L. Huang, H. Chen, Q. Li, Catal. Lett. 55 (1998) 157–163.
[41] I.V. Kozhevnikov, K.R. Kloetstra, A. Sinnema, H.W. Zandbergen, H. van Bekkum, J. Mol. Catal. A: Chem. 114 (1996) 287–298.
[42] V.K. Díez, C.R. Apesteguía, J.I. Di Cosimo, Catal. Today 149 (2010) 267–274.
[43] E. Modrogan, M.H. Valkenberg, W.F. Hoelderich, J. Catal. 261 (2009) 177–187.
[44] M. Hara, Top. Catal. 53 (2010) 805–810.
[45] C.L. Padró, E.A. Rey, L.F. González Peña, C.R. Apesteguía, Microporous Mesoporous Mater. 143 (2011) 236–242.
[46] N. Lavaud, P. Magnoux, F. Alvarez, L. Melo, G. Giannetto, M. Guisnet, J. Mol. Catal. A: Chem. 142 (1999) 223–236.
[47] C.H. Bartholomew, Appl. Catal. A: Gen. 212 (2001) 17–60.
[48] L. Palumbo, F. Bonino, P. Beato, M. Bjørgen, A. Zecchina, S. Bordiga, J. Phys. Chem. C 112 (2008) 9710–9716.
[49] C.E. Webster, R.S. Drago, M.C. Zerner, J. Phys. Chem. B 103 (1999) 1242–1249.
[50] S. Cai, K. Sohlberg, J. Mol. Catal. A: Chem. 193 (2003) 157–164.
[51] V.K. Diez, C.R. Apesteguía, J.I. Di Cósimo, J. Catal. 215 (2003) 220–233.
[52] G. Larsen, E. Lotero, L.M. Petkovic, D.S. Shobe, J. Catal. 169 (1997) 67–75.
[53] B. Shi, B.H. Davis, J. Catal. 157 (1995) 359–367.
[54] C. Baerlocher, W.M. Meier, D.H. Olson, Atlas of Zeolite Framework Types, fifth revised Ed., Elsevier, Amsterdam, 2001.
[55] J.W. Park, S.J. Kim, M. Seo, S.Y. Kim, Y. Sugi, G. Seo, Appl. Catal. A: Gen. 349 (2008) 76–85.